Continuum Mech. Thermodyn. (2020) 32:693–708
https://doi.org/10.1007/s00161-018-0709-8

ORIGINAL ARTICLE

B. Emek Abali · **Felix A. Reich**

Verification of deforming polarized structure computation by using a closed-form solution

Received: 11 February 2018 / Accepted: 3 September 2018 / Published online: 14 September 2018

Abstract Various engineering systems exploit the conversion between electromagnetic and mechanical work. It is important to compute this coupling accurately, and we present a method for solving the governing equations simultaneously (at once) without a staggering scheme. We briefly present the theory for coupling the elecgoverning equations as well as the variational formulation that leads to the weak form. This weak form is nonlinear and couples various fields. In order to solve the weak form, we use the finite element method in space and the finite difference method in time for the discretization of the computational domain. Numerical problems are circumvented by selecting the field equations carefully, and the weak form is assembled using standard shape functions. In order to examine the accuracy of the method, for the case of a linear elastic material under small deformations, we present and use an analytic solution. Comparison of the computation to the closed-form solution shows that the computational approach is reliable and models the jump of the electromagnetic fields across the interface between two different materials.

Keywords Mechanics · Electromagnetism · Finite element method

1 Introduction

Engineering applications, for example micro-electro-mechanical systems (MEMS), generate mechanical work as a consequence of the applied electromagnetic fields, or vice versa. This mechanism is used in many devices, a typical application is a vibrating smartphone. We aim at an accurate simulation of this mechanism by involving the correct coupling between mechanics and electromagnetism. As easily stated, the correct coupling is quite challenging and there is a long debate in the literature known as the ABRAHAM–MINKOWSKI controversy. In simpler words, we fail to know the correct modeling of the interaction between electromagnetism and mechanics. There exists no consensus in the scientific community, see for example [8,11,26,34,38]. We will use a possible modeling scenario and emphasize that different choices are admissible as well.

Computation of electromagnetism is actively discussed in the literature. Starting with [37,41], MAXWELL's equations are solved by using finite element methods with mixed elements. Different strategies are developed as in [12,13], [18, Sect. 17], [22,31]. Several strategies denote the lack of a general approach for solving electromagneto-mechanics problems. Mixed elements are useful to circumvent numerical problems. However, their generalization to multiphysics problems is very challenging. There exist various element types [6], and it is not clear, which type works fine for a specific type of application. Often, we simply do not know how to

Communicated by Francesco dell'Isola.

B. E. Abali (✉) · F. A. Reich
Chair of Continuum Mechanics and Constitutive Theory, Institute of Mechanics, Technische Universität Berlin, Einsteinufer 5, 10587 Berlin, Germany
E-mail: bilenemek@abali.org
URL: http://bilenemek.abali.org

choose the suitable mixed element. Therefore, some alternatives are emerging that employ alternative methods as in [19,20,24,40,45]. A finite element method is applied in [2, Chap. 3] by using "standard" continuous GALERKIN elements. The most remarkable benefit of this approach relies on the use of standard elements such that an extension to multiphysics problem is straightforward.

Commercial softwares use staggered schemes for solving coupled problems. A staggered scheme is effective and reliable, if the coupling between the fields is small. Multiphysics simulations—in the case of a strong coupling—necessitates a monolithic solution procedure, in other words, the governing equations need to be solved at once. There are various procedures and computational strategies for solving applications, which make use of the conversion between electric and mechanical work as in [5,23,48]. Especially for MEMS, even structural properties can be incorporated [7,16,17]. In such a complex model, corresponding material models are characterized by several material parameters, for a discussion of their determination, see [15,35,39,46]. For transient systems, computational implementation of an electromagneto-mechanical problem is also discussed in the literature; there are various techniques to obtain a robust strategy as in [1,40]. For a detailed review about computational methods, we refer to [10,28,47].

In this work we follow the theory and the computational strategy as in [4]. First, we briefly present the theory. There are open questions in developing a successful coupling between mechanics and electromagnetism. We will point out the key issues and generate the governing equations for a specific case of an application, where a steel sphere deforms under an externally applied magnetic field. Secondly, we compute the solution of this application. The coupling between mechanics and electromagnetism is bidirectional, and its quantification depends on the definition of the electromagnetic force. Thirdly, for this simple geometry, we will obtain a closed-form solution by following [42]. We exploit this analytic solution in order to examine the validity of the computational approach. All computations are established by using open-source packages and the codes are made publicly available in [3] under the GNU public license as in [25].

2 Governing equations for the theory of electromagnetism with deforming solids

The objective is to compute the displacement $\boldsymbol{u}$ in m, the electric field $\boldsymbol{E}$ in V/m, and the magnetic flux (area density) $\boldsymbol{B}$ in T as vector functions in space $\boldsymbol{x} \in \mathbb{R}^3$ and time $t \in [0, t_{\text{end}}]$. All these fields are (indirectly) measurable quantities. We assume a priori an isothermal system such that the temperature deviation from the reference state is neglected. For various applications, especially in the case of small elastic deformations, this assumption is applicable. Moreover, the displacement will be small such that we neglect geometric nonlinearities. Thus, $\boldsymbol{x}$ indicates the particle and this configuration is called the LAGRANGEan frame in continuum mechanics. In other words, $\boldsymbol{x}$ denotes the position of a particle in a reference frame, mostly chosen as the initial state. Hence, other common names are initial configuration or placement. The assumption of small deformations is used in two ways. First, the transformation of electromagnetic fields to the reference frame is circumvented. This point is crucial as there is no consensus in the scientific community on the transformation properties for electromagnetic fields between the current and the reference frame. Secondly, neglecting the geometric nonlinearities and choosing a linear elastic material model lead to a linear partial differential equation for the displacement field. An analytic solution of such a field equation is possible, depending on the problem.

All fields are expressed in Cartesian coordinates; we mostly use the index notation with indices i, j, k, l going from 1 to 3 in $\mathbb{R}^3$ with EINSTEIN's summation convention over repeated indices, and $_{,i}$ is used for partial derivatives in x_i. By using the FARADAY law and the motivation as in [36, Chap. 9], we obtain two MAXWELL equations that incorporate the electric field and the magnetic flux. Their solution is possible by the electric potential ϕ in V and the magnetic potential $\boldsymbol{A}$ in T m with the following ansatz functions:

$$E_i = -\phi_{,i} - \frac{\partial A_i}{\partial t}, \quad B_i = \epsilon_{ijk} A_{k,j}, \tag{1}$$

where the LEVI-CIVITA symbol, ϵ_{ijk}, is used that is the permutation symbol in Cartesian coordinates. Instead of computing the electromagnetic fields $\boldsymbol{E}$ and $\boldsymbol{B}$, we will compute the electromagnetic potentials ϕ and $\boldsymbol{A}$ that lead to the electric field and the magnetic flux in post-processing. These four ansatz functions in Eq. (1) introduce two relations in order to define the six electromagnetic fields $\boldsymbol{E}$ and $\boldsymbol{B}$ in $\mathbb{R}^3$ uniquely. These two relations are the rate of the electric potential and divergence of the magnetic potential. As they can be chosen arbitrarily, this is called gauge freedom. Their choice affects the electromagnetic potentials; however, not the

measurable electromagnetic quantities. As also suggested in [9], for the sake of the numerical robustness, we use the LORENZ gauge:

$$\frac{\partial \phi}{\partial t} = -c^2 A_{i,i}\,, \quad \text{with } c^2 = \frac{1}{\mu_0 \varepsilon_0} \tag{2}$$

being the square of the speed of light in the vacuum, c, and the universal constants:

$$\varepsilon_0 = 8.85 \times 10^{-12}\,\mathrm{A\,s/(V\,m)}\,, \quad \mu_0 = 12.6 \times 10^{-7}\,\mathrm{V\,s/(A\,m)}. \tag{3}$$

A particle with an electric charge in C has a mass in kg as well. Therefore, we introduce mass density ρ in kg/m^3 and specific charge z in C/kg in order to write out the balance of electric charge:

$$\frac{\partial \rho z}{\partial t} + J_{i,i} = 0, \tag{4}$$

with an electric current (area) density $\boldsymbol{J}$ in A/m^2 to be defined. By using an analog argumentation as before and introducing the so-called charge potential $\boldsymbol{D}$ in C/m^2 and the current potential $\boldsymbol{H}$ in A/m, we obtain the following MAXWELL equations:

$$\rho z = D_{i,i}\,, \quad \frac{\partial D_j}{\partial t} = \epsilon_{jkl} H_{l,k} - J_j. \tag{5}$$

These fields are related to the measurable fields by the experimentally verified MAXWELL–LORENTZ aether relations:

$$D_i = \varepsilon_0 E_i\,, \quad H_i = \frac{1}{\mu_0} B_i. \tag{6}$$

These relations hold universally in inertial frames, i.e., for any matter or even without (in vacuum). The charge and current potentials are caused by moving charges. Charge can be decomposed into free charge and bound charge. The free charges are, e.g., valence electrons moving in macroscopic distances. Bound charges are bound to the molecular configuration, and they move in atomic distances. These phenomena happen in different length scales such that we decompose the total charge potential, $\boldsymbol{D}$, into free charge potential, $\mathfrak{D}$, and bound charge potential, $\boldsymbol{P}$, as well as the total current potential, $\boldsymbol{H}$, into free current potential, $\mathfrak{H}$, and bound current potential, $\boldsymbol{\mathcal{M}}$, additionally, in analogous way the total electric current into free and bound terms as follows:

$$\begin{aligned} D_i &= \mathfrak{D}_i - P_i\,, \quad H_i = \mathfrak{H}_i + \mathcal{M}_i, \\ J_i &= J_i^{\mathrm{fr.}} + \frac{\partial P_i}{\partial t} + \epsilon_{ijk} \mathcal{M}_{k,j}. \end{aligned} \tag{7}$$

The electric current $\boldsymbol{J}^{\mathrm{fr.}}$ is the effective free electric current. Since we have the MAXWELL–LORENTZ aether relations as in Eq. (6), either the free charge and current potentials $\mathfrak{D}$, $\mathfrak{H}$, or the so-called electric and magnetic polarizations, $\boldsymbol{P}$, $\boldsymbol{\mathcal{M}}$, need to be defined by appropriate constitutive equations.

For the computation of the electric potential, ϕ, we use Eqs. (4) and $(5)_1$. For obtaining the magnetic potential, $\boldsymbol{A}$, after a straightforward derivation incorporating Eqs. $(5)_2$ and (2), we obtain

$$\varepsilon_0 \frac{\partial^2 A_i}{\partial t^2} - \frac{1}{\mu_0} A_{i,kk} - J_i = 0, \tag{8}$$

see [2, Sect. 3.2] for a detailed derivation. We model the electromagnetic potentials as smooth functions. However, the electric and magnetic polarizations have jumps on the interface between different materials—the effect of this is also observed in the resulting electromagnetic field, i.e., in the derivatives of the potentials. By neglecting surface charges and currents, we obtain

$$[\![n_i P_i]\!] = 0\,, \quad [\![\epsilon_{ijk} n_j \mathcal{M}_k]\!] = 0, \tag{9}$$

where the jump brackets indicate the differences between the limiting values from both sides of an interface. The surface normal, n_i, as well as the LEVI-CIVITA symbol, ϵ_{ijk}, we will take out of the jump brackets since they are continuous functions. These jump conditions are going to be used in the variational formulation.

In order to compute the displacement field, $\boldsymbol{u}$, the balance of linear momentum is used,

$$\rho \frac{\partial^2 u_i}{\partial t^2} - \sigma_{ji,j} - \rho f_i = \mathcal{F}_i, \tag{10}$$

where the mass density, ρ in kg/m^3, is constant (in time) and given a priori; the stress tensor, $\boldsymbol{\sigma}$ in N/m^2, has to be defined by a constitutive equation; the specific force, $\boldsymbol{f}$ in N/kg, is due to gravitation and its numerical value is given. From the balance on singular surfaces (without mass), we obtain the continuity of stress tensor along the surface normal. Mechanical momentum has a production term, an electromagnetic force density, $\boldsymbol{\mathcal{F}}$, generated by the electromagnetic field. Therefore, mechanical momentum is not a conserved quantity. In a formal way, we can write the following relation:

$$\frac{\partial \mathcal{G}_i}{\partial t} = m_{ji,j} - \mathcal{F}_i, \tag{11}$$

for any tensor of rank, herein $\boldsymbol{\mathcal{F}}$. We realize that $\boldsymbol{\mathcal{G}}$ has the unit of momentum and $\boldsymbol{m}$ has the unit of stress. We need to define the electromagnetic momentum, $\boldsymbol{\mathcal{G}}$, and then choose the electromagnetic stress, $\boldsymbol{m}$, and the electromagnetic force density, $\boldsymbol{\mathcal{F}}$, in a way that Eq. (11) is satisfied. This approach is very useful in order to classify the ambiguity about the "proper choice" of the electromagnetic momentum. Hence, this strategy is used by many scientific groups, see for example [32, Eq. (15)], [30, Chap. 1], [14, Chap. XIV], [27, Chap. 8], [33, Sect. 3.3]. Unfortunately, the correct choice of the electromagnetic momentum is unknown, for various possibilities we refer to [8,11,26,34,38]. A detailed discussion is found in [21] as well as in [44]. A thorough investigation of different possible choices can be found in [43]. Nevertheless, by inserting the identity in Eq. (11) into Eq. (10), we obtain the balance of total momentum:

$$\rho \frac{\partial^2 u_i}{\partial t^2} + \frac{\partial \mathcal{G}_i}{\partial t} - \left(\sigma_{ji} + m_{ji}\right)_{,j} - \rho f_i = 0\,, \quad n_j [\![\sigma_{ji} + m_{ji}]\!] = 0, \tag{12}$$

where the first two terms are the rate of the total momentum and $\sigma_{ji} + m_{ji}$ is the total momentum flux. Total momentum is a conserved quantity since no production terms arise. In order to complete the definition, we need to choose an electromagnetic momentum. We use the following electromagnetic momentum:

$$\mathcal{G}_i = (\mathfrak{D} \times \boldsymbol{B})_i, \tag{13}$$

which is called Minkowski's momentum. After using the Maxwell equations and Maxwell–Lorentz aether relations, we obtain the following electromagnetic stress and force density:

$$\begin{aligned} m_{ji} &= -\frac{1}{2}\delta_{ji}(H_k B_k + D_k E_k) + H_i B_j + D_j E_i, \\ \mathcal{F}_i &= \rho z E_i + \epsilon_{ijk} J_j B_k - \epsilon_{ijk} \frac{\partial P_j}{\partial t} B_k - \epsilon_{ijk} P_j \frac{\partial B_k}{\partial t}. \end{aligned} \tag{14}$$

It can be noted that these definitions are not unique, even though the momentum density is fixed. It is always possible to move parts of the force to the stress, and vice versa. After choosing the electromagnetic momentum, the production term in Eq. (10) can be exchanged by Eq. (11) such that no production terms arise for the total momentum density, which is the mechanical momentum and the electromagnetic momentum. Hence, the total momentum is a conserved quantity.

Summing up, we employ the primitive variables $\{\boldsymbol{u}, \phi, \boldsymbol{A}\}$ that need to satisfy Eqs. (5), (8), (9), (10) called the governing equations:

$$\begin{aligned} &\rho \frac{\partial^2 u_i}{\partial t^2} - \sigma_{ji,j} - \rho f_i = \mathcal{F}_i\,, \quad \frac{\partial D_{i,i}}{\partial t} + J_{i,i} = 0\,, \quad \varepsilon_0 \frac{\partial^2 A_i}{\partial t^2} - \frac{1}{\mu_0} A_{i,kk} - J_i = 0, \\ &n_i [\![P_i]\!] = 0\,, \quad \epsilon_{ijk} n_j [\![\mathcal{M}_k]\!] = 0\,, \quad n_j [\![\sigma_{ji}]\!] = -n_j [\![m_{ji}]\!], \end{aligned} \tag{15}$$

with Eqs. (2), (7), $(14)_2$. We rewrite Eq. $(14)_2$ by using the Maxwell equation $(7)_3$, and tensor identities, as follows

$$\mathcal{F}_i = \rho z E_i + \epsilon_{ijk} J_j B_k - \epsilon_{ijk} \frac{\partial P_j}{\partial t} B_k - \epsilon_{ijk} P_j \frac{\partial B_k}{\partial t} = D_{j,j} E_i + \epsilon_{ijk} J^{\text{fr.}}_j B_k + \epsilon_{ijk} \epsilon_{jlm} \mathcal{M}_{m,l} B_k - \epsilon_{ijk} P_j \frac{\partial B_k}{\partial t}. \tag{16}$$

After defining $\boldsymbol{\sigma}$, $\boldsymbol{J}^{\text{fr.}}$, $\boldsymbol{P}$, $\boldsymbol{\mathcal{M}}$, we can solve the governing equations.

For a special case of a polarized but conducting isotropic material, i.e., no piezoelectric or piezomagnetic character is present because of the crystallographic structure, the linear constitutive equations are as follows:

$$\sigma_{ij} = C_{ijkl} \varepsilon_{kl}\,, \quad \varepsilon_{ij} = u_{(i,j)} = \frac{1}{2}\left(u_{i,j} + u_{j,i}\right), \quad C_{ijkl} = \lambda \delta_{ij} \delta_{kl} + \mu \delta_{ik} \delta_{il} + \mu \delta_{il} \delta_{jk},$$

$$P_i = \varepsilon_0 \chi^{\text{el}} E_i \ , \quad \mathcal{M}_i = \frac{\chi^{\text{mag}}}{\mu^{\text{mag}}} B_i \ , \quad J_i^{\text{fr.}} = \mathcal{J}_i^{\text{fr.}} + \rho z^{\text{fr.}} v_i ,$$
$$\rho z^{\text{fr.}} = \mathfrak{D}_{i,i} \ , \quad \mathcal{J}_i^{\text{fr.}} = \varsigma \mathcal{E}_i \ , \quad \mathcal{E}_i = E_i + \epsilon_{ijk} v_j B_k \ , \quad v_i = \frac{\partial u_i}{\partial t} \ , \tag{17}$$

where we have neglected a possible magnetoelectric coupling as well as employed a linearized strain measure as a consequence of the small displacements. We refer to the thermodynamical formulation in [4] for deducing these equations. Herein, all material parameters are constant: the electric susceptibility, χ^{el}, the magnetic susceptibility, χ^{mag}, the permeability $\mu^{\text{mag}} = \mu_r \mu_0$, with the relative permeability, $\mu_r = \chi^{\text{mag}} + 1$, the mechanical moduli λ, μ, as well as the electric conductivity, ς. The permittivity ε_0 and permeability μ_0 of the vacuum are universal constants.

3 Generating the weak form

The governing equations (15) need to be satisfied in every point locally such that we can use the so-called weighted residuals in a domain Ω with its boundary $\partial\Omega$. The domain can be chosen as the whole continuum body or also only a part of it. By choosing the domain a finite size element and approximating unknowns $\{\boldsymbol{u}, \phi, \boldsymbol{A}\}$ as expanded with form (shape) functions in this domain, we implement the finite element method. We emphasize that we choose in each element Ω to fulfill the weighted residuals with functions expanded in a HILBERTian SOBOLEV space such that their differentiability and square integrability is assured by using "standard" linear LAGRANGE form functions:

$$\mathcal{V} = \left\{ \{\boldsymbol{u}, \phi, \boldsymbol{A}\} \in [\mathcal{H}^1(\Omega)]^7 : \{\boldsymbol{u}, \phi, \boldsymbol{A}\}\Big|_{\partial\Omega} = \text{given} \right\}, \tag{18}$$

for 3 displacements and 4 electromagnetic potentials in 3D space. Especially in electromagnetism, this choice is uncommon; however, we emphasize that we solve the electromagnetic potentials instead of electromagnetic fields and employ the LORENZ gauge. As a consequence, no numerical problems arise even in the case of using standard elements.

In order to generate the weighted residuals, the right-hand side is subtracted from the left-hand side and then multiplied by the corresponding test function. Equations $(15)_{1,3}$ are rank one tensor equations, hence vector-valued test functions are employed. Equation $(15)_2$ is a rank zero tensor equation, the chosen test function is scalar. As usual in GALERKIN's approach, we use the same space for expanding the unknowns as well as their test functions. For reducing the differentiability condition, we use partial integration on all terms including derivatives of second order and obtain the following weak forms in every finite element,

$$\begin{aligned}
F_{\boldsymbol{u}}^{\text{ele}} &= \int_\Omega \left(\rho \frac{\partial^2 u_i}{\partial t^2} \delta u_i + \sigma_{ji} \delta u_{i,j} - \rho f_i \delta u_i - \mathcal{F}_i \delta u_i \right) \mathrm{d}V - \int_{\partial\Omega} n_j \sigma_{ji} \delta u_i \, \mathrm{d}A , \\
F_{\phi}^{\text{ele}} &= \int_\Omega \Big(- \frac{\partial \mathfrak{D}_i}{\partial t} \delta\phi_{,i} - J_i^{\text{fr.}} \delta\phi_{,i} - \epsilon_{ijk} \mathcal{M}_{k,j} \delta\phi_{,i} \Big) \mathrm{d}V + \int_{\partial\Omega} n_i \Big(\frac{\partial \mathfrak{D}_i}{\partial t} + J_i^{\text{fr.}} + \epsilon_{ijk} \mathcal{M}_{k,j} \Big) \delta\phi \, \mathrm{d}A , \\
F_{\boldsymbol{A}}^{\text{ele}} &= \int_\Omega \left(\varepsilon_0 \frac{\partial^2 A_i}{\partial t^2} \delta A_i + \frac{1}{\mu_0} A_{i,j} \delta A_{i,j} - J_i^{\text{fr.}} \delta A_i - \frac{\partial P_i}{\partial t} \delta A_i + \epsilon_{ijk} \mathcal{M}_k \delta A_{i,j} \right) \mathrm{d}V \\
&\quad + \int_{\partial\Omega} n_j \Big(\frac{1}{\mu_0} A_{i,j} + \epsilon_{ijk} \mathcal{M}_k \Big) \delta A_i \, \mathrm{d}A .
\end{aligned} \tag{19}$$

All these forms are valid within a single finite element in a material. The whole computational domain possesses various materials. If we sum over all finite elements within the domain, the materials properties are discontinuous at some element surfaces, we insert the jump conditions as in Eq. (15). We emphasize that all unknowns are continuous, even across any interface, $\partial\Omega^I$, between different materials. On the boundary of the domain, the values of the unknowns are given by DIRICHLET boundary conditions such that the test functions vanish. For the time discretization, we use the finite difference method and obtain the unknowns in a list of instants, $t = \{0, \Delta t, 2\Delta t, 3\Delta t, \dots\}$, by using a time step, Δt. The time step is constant and has to be chosen small enough such that the NEWTON–RAPHSON iteration converges to the solution. We apply an EULER backwards scheme in time and acquire

$$F_{\boldsymbol{u}} = \sum_{\text{ele}} \int_\Omega \left(\rho \frac{u_i - 2u_i^0 + u_i^{00}}{\Delta t^2} \delta u_i + \sigma_{ji} \delta u_{i,j} - \rho f_i \delta u_i - \mathcal{F}_i \delta u_i \right) \mathrm{d}V + \int_{\partial\Omega^I} n_j [\![m_{ji}]\!] \delta u_i \, \mathrm{d}A ,$$

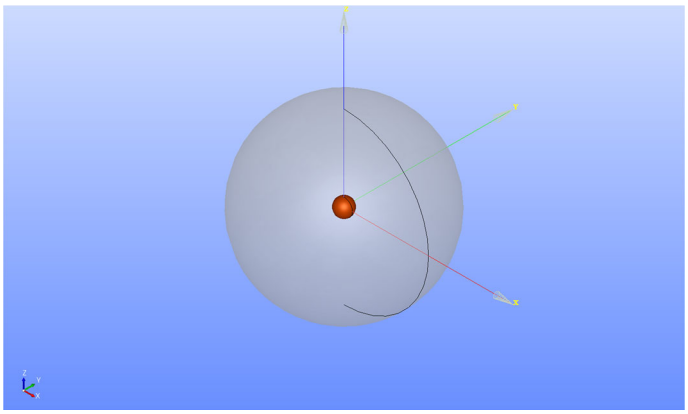

Fig. 1 Computational domain consisting of a steel sphere (orange), embedded in air (transparent, gray) (color figure online)

$$
\begin{aligned}
F_\phi &= \sum_{\text{ele}} \int_\Omega \Big(-(\mathfrak{D}_i - \mathfrak{D}_i^0)\delta\phi_{,i} - \Delta t\, J_i^{\text{fr.}}\delta\phi_{,i} - \Delta t \epsilon_{ijk}\mathcal{M}_{k,j}\delta\phi_{,i}\Big)\,\mathrm{d}V \\
&\quad + \int_{\partial\Omega^I} \Delta t n_i \big([\![J_i^{\text{fr.}}]\!] + \epsilon_{ijk}[\![\mathcal{M}_{k,j}]\!]\big)\delta\phi\,\mathrm{d}A, \\
F_{\boldsymbol{A}} &= \sum_{\text{ele}} \int_\Omega \left(\varepsilon_0 \frac{A_i - 2A_i^0 + A_i^{00}}{\Delta t^2}\delta A_i + \frac{1}{\mu_0} A_{i,j}\delta A_{i,j} - J_i^{\text{fr.}}\delta A_i - \frac{P_i - P_i^0}{\Delta t}\delta A_i + \epsilon_{ijk}\mathcal{M}_k \delta A_{i,j} \right) \mathrm{d}V,
\end{aligned}
\tag{20}
$$

discrete in time, where $(\cdot)^0$ denotes the numerical value that was computed at the last instant, $t - \Delta t$. All the integral forms are brought to the same unit of energy such that we can sum them up, $F = F_{\boldsymbol{u}} + F_\phi + F_{\boldsymbol{A}}$ and set the objective to determine the variables satisfying the weak form F.

4 Application

Consider an isotropic and in each aspect linear material that is modeled by the constitutive equations (17). To demonstrate, we use the parameters for steel. As the geometry, a sphere (of steel) is considered, which is embedded in an outer sphere (of air), as seen in Fig. 1. The radius of the steel sphere is $R = 0.1\,\text{m}$, and of the outer embedding air sphere it is 1 m. In the analytic solution, the outer radius is set to infinity to construct a perfect exterior domain. For the numerical solution, ten times the radius of the steel sphere is sufficient, in practice, for approximating the boundary as a far-field boundary. An external, homogeneous magnetic field is set as the far-field condition, with magnitude B_0. Since the air is not polarized, we can also define $\mathfrak{H}_0 = H_0 = \mu_0^{-1} B_0$, in the z direction. No exterior pressure nor any magnetic distortion due to the surroundings are considered. We present the analytical solution in the following for determining the accuracy of the numerical model.

4.1 Analytical reference problem

In order to test the numerical scheme, a closed-form solution to the aforementioned application is developed. The electric polarization, $\boldsymbol{P}$, and the effective current, $\boldsymbol{\jmath}^{\text{fr.}}$, are set to zero. Also, there are no free charges in the body. The constitutive equations (17) are used. As the constitutive laws are not coupled in this problem, it is possible to separate the involved mechanical and electromagnetic parts of the problem. The magnetic problem is solved first, and, using the obtained results, the electromagnetic force distribution is determined which is needed to obtain the displacement field for the static problem. The analytic solution of the presented problem is adapted from [42], where the derivation is shown in a detailed manner. Here, we explain the key points and give a brief overview of the method.

By using all simplifications, it is possible to introduce a scalar potential for the magnetic field because the curl of the free current potential vanishes. This fact is seen by starting with Eq. $(5)_2$ and inserting Eq. (7) for

obtaining the so-called material MAXWELL's equations. As both the free current density as well as the time derivative of the free charge potential vanish, we realize that the curl of the free current potential has to be zero as well. In the end, we obtain

$$\nabla \times \mathfrak{H} = 0. \tag{21}$$

Furthermore, the free current potential $\mathfrak{H}_i$ is decomposed into the distortion field $\hat{\mathfrak{H}}_i$ (due to the magnetic properties of the sphere) and the external field $\mathfrak{H}_i^0$ as follows

$$\mathfrak{H}_i = \hat{\mathfrak{H}}_i + \mathfrak{H}_i^0. \tag{22}$$

In order to satisfy Eq. (21), we use a distortion field as $\hat{\mathfrak{H}}_i = -V^{\mathrm{M}}_{,i}$ by a scalar potential V^{M}. As the magnetic flux must be solenoidal, LAPLACE equation is obtained,

$$\Delta V^{\mathrm{M}} = 0, \tag{23}$$

for V^{M}—valid both inside as well as outside of the sphere. Normal continuity of the magnetic flux density and tangential continuity of the free current potential can also be denoted in terms of the potential. We start with Eq. (9) and use Eq. $(17)_{4,5}$ and $\mathfrak{H}_i = \mu_{\mathrm{mag}}^{-1} B_i$ such that we obtain

$$[\![\varepsilon_0 \chi^{\mathrm{el}} E_i]\!] = 0\,, \quad \left[\!\!\left[\frac{1}{\mu^{\mathrm{mag}}} \epsilon_{ijk} n_j \mathfrak{H}_k \right]\!\!\right] = 0. \tag{24}$$

Thus, we obtain the following governing equations:

$$[\![V^{\mathrm{M}}]\!] = 0, \quad \text{and} \quad n_i [\![\mu_r V^{\mathrm{M}}_{,i}]\!] = n_i \mathfrak{H}_i^0 [\![\mu_r]\!]. \quad \text{Also,} \quad \lim_{r\to\infty} V^{\mathrm{M}} = 0 \tag{25}$$

to ensure that the magnetic field converges to the external field $\mathfrak{H}_i^0$. Outside of the sphere, the relative permeability is set to one as for vacuum, or, in good approximation, for air. In the following, μ_r refers to the value of the steel sphere. Due to the azimuthal symmetry of the problem, we introduce a spherical coordinate system, (r, ϑ, φ), where r denotes the distance to the origin, ϑ is the azimuthal angle, and φ gives the polar angle as follows:

$$r = \|x_i\| = \sqrt{(x_1^2 + x_2^2 + x_3^2)}\,, \quad \vartheta = \arccos\left(\frac{x_3}{\|x_i\|}\right), \quad \varphi = \arctan\left(\frac{x_2}{x_1}\right). \tag{26}$$

The corresponding base vectors read $\boldsymbol{e}_r$, $\boldsymbol{e}_\vartheta$, $\boldsymbol{e}_\varphi$. The solution of the LAPLACE equation can be expressed in spherical coordinates by

$$V^{\mathrm{M}}(\tilde{r}, \vartheta) = \sum_{n=0}^{\infty} \left(a_n \tilde{r}^n + b_n \tilde{r}^{-(n+1)} \right) P_n(\cos\vartheta). \tag{27}$$

In this series, P_n are LEGENDRE polynomials and $\tilde{r} = {}^{r}/_{R}$ is the dimensionless radial coordinate. By imposing a finiteness condition on V^{M} and by exploiting the limiting boundary condition, two functions are found for the potential: one that is valid within the sphere, $V^{\mathrm{M/I}}$, and one that is valid outside of it, $V^{\mathrm{M/O}}$. The coefficients are readily found by exploiting the jump conditions. Since the series degenerate in each domain and we obtain

$$V^{\mathrm{M/I}} = \frac{\mu_r - 1}{\mu_r + 2} \mathfrak{H}_0 R \tilde{r} \cos\vartheta, \quad \text{and} \quad V^{\mathrm{M/O}} = \frac{\mu_r - 1}{\mu_r + 2} \mathfrak{H}_0 R \tilde{r}^{-2} \cos\vartheta. \tag{28}$$

Hence, the fields $\boldsymbol{B}$ and $\mathfrak{H}$ are determined by using $\hat{\mathfrak{H}}_i = -V^{\mathrm{M}}_{,i}$ as well as by Eqs. (6), (7). We emphasize that both $\boldsymbol{B}$ and $\mathfrak{H}$ are homogeneous and constant fields within the sphere. For example, the magnetic flux reads with respect to the physical basis of spherical coordinates in both domains,

$$\begin{aligned} \boldsymbol{B}^{\mathrm{I}} &= \tfrac{3\mu_r}{2+\mu_r} \mu_0 \mathfrak{H}_0 (\cos\vartheta \boldsymbol{e}_r - \sin\vartheta \boldsymbol{e}_\vartheta) = \tfrac{3\mu_r}{2+\mu_r} \mu_0 \mathfrak{H}^0 \boldsymbol{e}_z, \\ \boldsymbol{B}^{\mathrm{O}} &= \tfrac{1}{2+\mu_r} \mu_0 \mathfrak{H}_0 \left(\left(2(\mu_r - 1)\tilde{r}^{-3} + 2 + \mu_r \right) \cos\vartheta \boldsymbol{e}_r + \left((\mu_r - 1)\tilde{r}^{-3} - 2 - \mu_r \right) \sin\vartheta \boldsymbol{e}_\vartheta \right). \end{aligned} \tag{29}$$

With these closed-form results, the electromagnetic force is determined. For the chosen MINKOWSKI force model, the regular electromagnetic force density reads in this steady-state problem

$$\mathcal{F}_i = m_{ij,j} = 0, \tag{30}$$

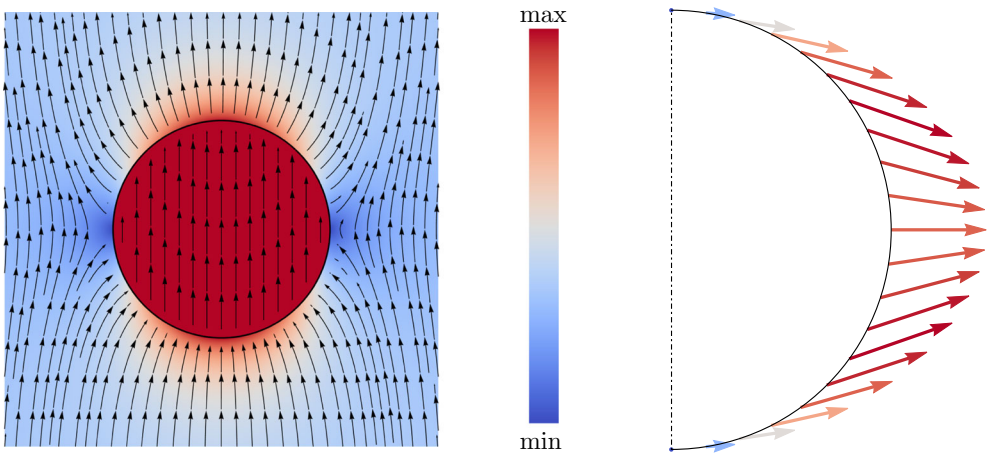

Fig. 2 Qualitative representations of the magnetic flux density and the resulting electromagnetic surface force distribution of the spherical reference problem. Colors indicate the magnitudes of the respective fields. The images are adapted from [42]. **a** Magnetic flux density $\boldsymbol{B}$. **b** Surface force $\boldsymbol{\mathcal{F}}^{(I)}$ (color figure online)

as the electromagnetic stress tensor is constant within the sphere due to the remarks of the last paragraph. Even though the regular force density vanishes, this is not the case on the singular surface,

$$\boldsymbol{\mathcal{F}}^{(I)} = \boldsymbol{n} \cdot [\![\boldsymbol{m}]\!] = (\boldsymbol{n} \times [\![\boldsymbol{\mathcal{M}}]\!]) \times \langle \boldsymbol{B} \rangle = \tfrac{9}{2} \tfrac{1}{(2+\mu_r)^2} \mu_0 \mathfrak{H}_0^2 [(\mu_r^2 - 1) \sin^2\vartheta \boldsymbol{e}_r + 2\mu_r(\mu_r - 1) \cos\vartheta \sin\vartheta \boldsymbol{e}_\vartheta]. \tag{31}$$

This force density acts on the surface of the sphere. The static momentum balance is solved within the sphere, using this force density as a boundary condition. The magnetic flux density of the problem and the resulting surface force distribution are visualized in Fig. 2.

For the static problem, the deformation due to the electromagnetic force is to be determined; gravitational body forces are neglected. As there is no regular electromagnetic force density, the momentum balance within the sphere domain reduces to the homogeneous NAVIER equations:

$$(\lambda + \mu) u_{j,ji} + \mu u_{i,jj} = 0. \tag{32}$$

For the case of azimuthal symmetry, this equation was analytically solved by HIRAMATSU and OKA in [29] by using series expansion. For the interior of a sphere, their solution for the physical components of the displacement field reads

$$u_r(\tilde{r}, \vartheta) = R \sum_{n=0}^{\infty} \left[-\frac{n\frac{\lambda}{\mu} + n - 2}{2(2n+3)} A_n \tilde{r}^{n+1} + n B_n \tilde{r}^{n-1} \right] P_n(\xi), \tag{33a}$$

$$u_\vartheta(\tilde{r}, \vartheta) = R \sum_{n=1}^{\infty} \left[-\frac{(n+3)\frac{\lambda}{\mu} + n + 5}{2(n+1)(2n+3)} A_n \tilde{r}^{n+1} + B_n \tilde{r}^{n-1} \right] \frac{\mathrm{d}P_n(\xi)}{\mathrm{d}\vartheta}, \tag{33b}$$

and, in this problem, $u_\varphi = 0$ due to the symmetry of the electromagnetic loading. In the latter equations, we have substituted $\xi = \cos\vartheta$ for the LEGENDRE polynomials $P_n(\xi)$. Their solution for the physical components of the CAUCHY stress reads

$$\sigma_{rr}(\tilde{r}, \vartheta) = \mu \sum_{n=0}^{\infty} \left[-\frac{(n^2 - n - 3)\frac{\lambda}{\mu} + (n+1)(n-2)}{2n+3} A_n \tilde{r}^n + 2n(n-1) B_n \tilde{r}^{n-2} \right] P_n(\xi), \tag{34a}$$

$$\sigma_{\vartheta\vartheta}(\tilde{r}, \vartheta) = \mu \sum_{n=0}^{\infty} \left[\frac{(n+3)\frac{\lambda}{\mu} - n + 2}{2n+3} A_n \tilde{r}^n + 2n B_n \tilde{r}^{n-2} \right] P_n(\xi)$$

$$+\mu\sum_{n=2}^{\infty}\left[-\frac{(n+3)\frac{\lambda}{\mu}+n+5}{(n+1)(2n+3)}A_n\tilde{r}^n+2B_n\tilde{r}^{n-2}\right]\frac{\mathrm{d}^2P_n(\xi)}{\mathrm{d}\vartheta^2}, \tag{34b}$$

$$\sigma_{\varphi\varphi}(\tilde{r},\vartheta)=\mu\sum_{n=0}^{\infty}\left[\frac{(n+3)\frac{\lambda}{\mu}-n+2}{2n+3}A_n\tilde{r}^n+2nB_n\tilde{r}^{n-2}\right]P_n(\xi)$$
$$+\mu\sum_{n=1}^{\infty}\left[-\frac{(n+3)\frac{\lambda}{\mu}+n+5}{(n+1)(2n+3)}A_n\tilde{r}^n+2B_n\tilde{r}^{n-2}\right]\frac{\mathrm{d}P_n(\xi)}{\mathrm{d}\vartheta}\cot(\vartheta), \tag{34c}$$

$$\sigma_{r\vartheta}(\tilde{r},\vartheta)=\mu\sum_{n=1}^{\infty}\left[-\frac{n(n+2)\frac{\lambda}{\mu}+n^2+2n-1}{(n+1)(2n+3)}A_n\tilde{r}^n+2(n-1)B_n\tilde{r}^{n-2}\right]\frac{\mathrm{d}P_n(\xi)}{\mathrm{d}\vartheta}, \tag{34d}$$

$$\sigma_{r\varphi}(\tilde{r},\vartheta)=\sigma_{\vartheta\varphi}(\tilde{r},\vartheta)=0. \tag{34e}$$

This solution satisfies the NAVIER equations. The coefficients A_n and B_n are determined from the singular momentum balance of interfaces, which reads in this problem

$$n_j[\![\sigma_{ji}]\!]=-\mathcal{F}_i^{(I)}\quad\Rightarrow\quad n_j\sigma_{ji}=\mathcal{F}_i^{(I)}, \tag{35}$$

as any exterior pressure is neglected. We use the convention that a jump bracket is evaluated as outside value subtracted by the inner value. Explicitly, one finds two non-trivial relations to be fulfilled,

$$\begin{aligned}\sigma_{rr}(\tilde{r}=1,\vartheta)&=\mathcal{F}_r^{(I)}(\vartheta),\\ \sigma_{r\vartheta}(\tilde{r}=1,\vartheta)&=\mathcal{F}_\vartheta^{(I)}(\vartheta).\end{aligned} \tag{36}$$

It can be seen that σ_{rr} depends on the LEGENDRE polynomials $P_n(\xi)$; the shear stress $\sigma_{r\vartheta}$ depends on derivatives of these polynomials, $\mathrm{d}P_n(\xi)/\mathrm{d}\vartheta$. Therefore, the radial surface force is expanded in $P_n(\xi)$ and the polar surface force is expanded in $\mathrm{d}P_n(\xi)/\mathrm{d}\vartheta$. Then, the coefficients are obtained algebraically and one finds that only few coefficients, A_n and B_n, remain,

$$\begin{aligned}A_0&=\frac{\mu_0\mathfrak{H}_0^2}{\mu}\hat{A}_0\,,\quad A_2=\frac{\mu_0\mathfrak{H}_0^2}{\mu}\hat{A}_2\,,\quad B_2=\frac{\mu_0\mathfrak{H}_0^2}{\mu}\hat{B}_2\,,\\ \hat{A}_0&=\frac{a}{\frac{\lambda}{\mu}+\frac{2}{3}}\,,\quad \hat{A}_2=\frac{21b-42c}{19\frac{\lambda}{\mu}+14}\,,\quad \hat{B}_2=\frac{(8\frac{\lambda}{\mu}+7)b+3\frac{\lambda}{\mu}c}{38\frac{\lambda}{\mu}+28}\,,\end{aligned} \tag{37}$$

with

$$a=3\frac{\mu_r^2-1}{(2+\mu_r)^2}\,,\quad b=-3\frac{\mu_r^2-1}{(2+\mu_r)^2}\,,\quad c=-3\frac{\mu_r(\mu_r-1)}{(2+\mu_r)^2}, \tag{38}$$

we refer to [42, Sect. 4.4] for their detailed derivation. Thus, the displacements read

$$\begin{aligned}u_r(\tilde{r},\vartheta)&=\tfrac{\mu_0\mathfrak{H}_0^2R}{\mu}\Big[\tfrac{1}{3}\hat{A}_0+\Big(2\hat{B}_2-\tfrac{1}{7}\tfrac{\lambda}{\mu}\hat{A}_2\tilde{r}^2\Big)P_2(\xi)\Big]\tilde{r},\\ u_\vartheta(\tilde{r},\vartheta)&=\tfrac{\mu_0\mathfrak{H}_0^2R}{\mu}\Big[\hat{B}_2-\tfrac{1}{42}\Big(5\tfrac{\lambda}{\mu}+7\Big)\hat{A}_2\tilde{r}^2\Big]\tilde{r}\frac{\mathrm{d}P_2(\xi)}{\mathrm{d}\vartheta}.\end{aligned} \tag{39}$$

The second LEGENDRE polynomial and its derivative,

$$P_2(\xi)=\frac{1}{2}\big(3\xi^2-1\big)\,,\quad \frac{\mathrm{d}P_2(\xi)}{\mathrm{d}\vartheta}=-3\xi\sqrt{1-\xi^2}, \tag{40}$$

indicate that there is only a radial displacement since the derivative vanishes effected by $\xi=\cos(\theta=\pi/2)=0$ along x-axis and $\xi=\cos(\theta=0)=1$ along z-axis. The deformed form of the body is determined and qualitatively illustrated in Fig. 3. The physical components of the stress follow as

$$\sigma_{rr}(\tilde{r},\vartheta)=\mu_0\mathfrak{H}_0^2\Big[\Big(\tfrac{2}{3}+\tfrac{\lambda}{\mu}\Big)\hat{A}_0+\Big(4\hat{B}_2+\tfrac{1}{7}\tfrac{\lambda}{\mu}\hat{A}_2\tilde{r}^2\Big)P_2(\xi)\Big], \tag{41a}$$

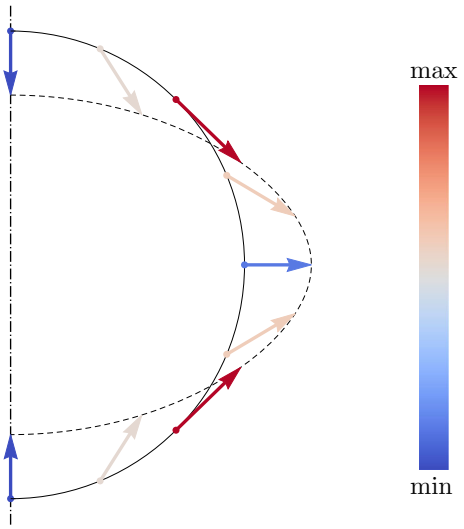

Fig. 3 Visualization of the surface displacement of the spherical reference problem. The color of the arrows indicates the magnitude of the displacements. The dashed line shows, qualitatively, the deformed form of the body. The image is adapted from [42] (color figure online)

$$\sigma_{\vartheta\vartheta}(\tilde{r},\vartheta)=\mu_0\mathfrak{H}_0^2\Big[\left(\tfrac{2}{3}+\tfrac{\lambda}{\mu}\right)\hat{A}_0+\left(4\hat{B}_2+\tfrac{5}{7}\tfrac{\lambda}{\mu}\hat{A}_2\tilde{r}^2\right)P_2(\xi)+\left(2\hat{B}_2-\left(\tfrac{1}{3}+\tfrac{5}{21}\tfrac{\lambda}{\mu}\right)\hat{A}_2\tilde{r}^2\right)\frac{\mathrm{d}^2P_2(\xi)}{\mathrm{d}\vartheta^2}\Big], \tag{41b}$$

$$\sigma_{\varphi\varphi}(\tilde{r},\vartheta)=\mu_0\mathfrak{H}_0^2\Big[\left(\tfrac{2}{3}+\tfrac{\lambda}{\mu}\right)\hat{A}_0+\left(4\hat{B}_2+\tfrac{5}{7}\tfrac{\lambda}{\mu}\hat{A}_2\tilde{r}^2\right)P_2(\xi)+\left(2\hat{B}_2-\left(\tfrac{1}{3}+\tfrac{5}{21}\tfrac{\lambda}{\mu}\right)\hat{A}_2\tilde{r}^2\right)\cot\vartheta\frac{\mathrm{d}P_2(\xi)}{\mathrm{d}\vartheta}\Big], \tag{41c}$$

$$\sigma_{r\vartheta}(\tilde{r},\vartheta)=\mu_0\mathfrak{H}_0^2\Big[2\hat{B}_2-\left(\tfrac{1}{3}+\tfrac{8}{21}\tfrac{\lambda}{\mu}\right)\hat{A}_2\tilde{r}^2\Big]\frac{\mathrm{d}P_2(\xi)}{\mathrm{d}\vartheta}. \tag{41d}$$

When the displacement of the numerical solution matches the analytic solution, the stress distribution will be accurate as well. Therefore, we concentrate on a comparison between magnetic flux and displacement in the following.

4.2 Computation

For the finite element analysis, we use the same geometry and find the steady-state solution by computing the weak form in Eq. (20). We neglect the inertial terms in the balance of linear momentum as well as gravitational body force. For the electromagnetic fields, we use the more general form as in the weak form. In order to obtain a constant magnetic flux within the surrounding air, we employ the following boundary condition for $\boldsymbol{A}$ leading to a constant magnetic flux along x_3 as follows:

$$A_i=\begin{pmatrix}0\\ \mu_0\mathfrak{H}_0x_1\\ 0\end{pmatrix},\quad B_i=\epsilon_{ijk}A_{k,j}=\begin{pmatrix}0\\ 0\\ \mu_0\mathfrak{H}_0\end{pmatrix}. \tag{42}$$

Effected by this boundary condition, the model lacks symmetry planes and we have to compute the whole spherical geometry. For the computation of displacements, the sphere has to be fixed such that any rigid body motion is suppressed. The appropriate choice of such a boundary condition is challenging since in the closed-form solution we do not consider this condition at all. We clamp in the middle of the steel sphere all points within the sphere of radius R_{BC} and present the effect in the following. As material parameters, realistic values for steel are employed as compiled in Table 1. The geometry is preprocessed in Salome with NetGen algorithms. The triangulation is made so that the steel sphere is composed of finer elements than the surrounding air. A cut view of the mesh is shown in Fig. 4. The computation is implemented in Python with

Table 1 Material constants used in the simulation for the steel and the surrounding air

		Steel	Air
Mass density	ρ in kg/m^3	7850	1.2
YOUNG's modulus	E in Pa	200×10^9	–
POISSON's ratio	ν	0.3	–
Modulus	λ in Pa	$\frac{E\nu}{(1+\nu)(1-2\nu)}$	0.1
Modulus	μ in Pa	$\frac{E}{2(1+\nu)}$	0.1
Electric susceptibility	χ^{el}	0	0
Magnetic susceptibility	χ^{mag}	100	0
Electric conductivity	ς in S/m	0	0

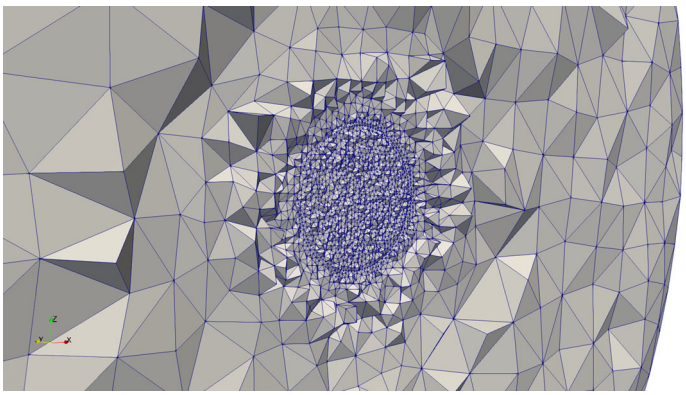

Fig. 4 The mesh is shown in a cut view. Within the steel sphere, the mesh is finer. Beyond the interface between the steel and air, the element size is increasing gradually. No special refinement for the interface is used

open-source codes developed by the FEniCS project.[1] Because of the high number of degrees of freedom, an iterative solver *bicgstab* with a preconditioner *hypre_amg* has been used in parallel computation.

4.3 Comparison

Almost the same application has been analyzed by a closed-form solution as well by an FEM computation. We consider the closed-form solution as the exact distribution, although the FEM computation incorporates both electromagnetic potentials as vector and scalar potentials without any assumption. Technically, FEM computation is more general; but we expect to converge toward exact solution. Hence, we set the objective as examining the accuracy of the FEM solution by comparing it to the exact solution. We emphasize that the FEM solution is obtained by solving the problem monolithically and transient in time by using standard linear FEM elements. By using the LORENZ gauge, we have eliminated several numerical problems. Moreover, the use of the hump conditions is of importance. We have used the same type of a jump condition for the numerical as well analytic solution by assuming that the total momentum flux along the surface normal is continuous. This assumption is taken for granted and its accuracy can only be determined by using experiments. Even though continuous elements are employed for the electromagnetic potentials, ϕ, $\boldsymbol{A}$, by employing the appropriate jump conditions, we expect accurate representations of jumps in the electromagnetic fields, $\boldsymbol{B}$, $\boldsymbol{E}$.

The solution of the magnetic flux is seen in Fig. 5, on top the distribution on plane is visualized in ParaView, on bottom the comparison is given of the vertical component along the radius by using MatPlotLib packages from SciPy.[2] The far away condition due to the domain boundary condition is fulfilled showing that 1 m surrounding air for 100 mm steel sphere is admissible. Without using any special elements on the interface, the jump of the magnetic flux is captured with a sufficient accuracy by using a relatively coarse mesh at the interface. Moreover, the distribution from the interface to the far-field condition is captured, even though the mesh is coarsening gradually along the radial direction. Within the sphere, only the external magnetic flux is

[1] The FEniCS computing platform, https://fenicsproject.org/.

[2] SciPy is a Python-based ecosystem of open-source software for science, https://www.scipy.org/.

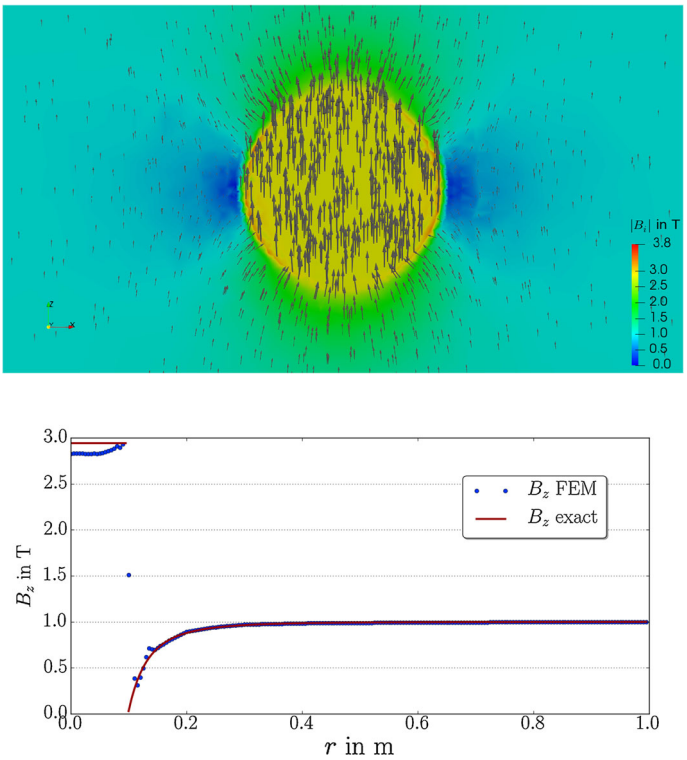

Fig. 5 FEM results: (top) magnetic flux distribution on a cut plane with scaled arrows, (bottom) comparison of the numerical solution along x-axis as dots to the closed-form solution along the radius at $\theta = \pi/2$ as a continuous line

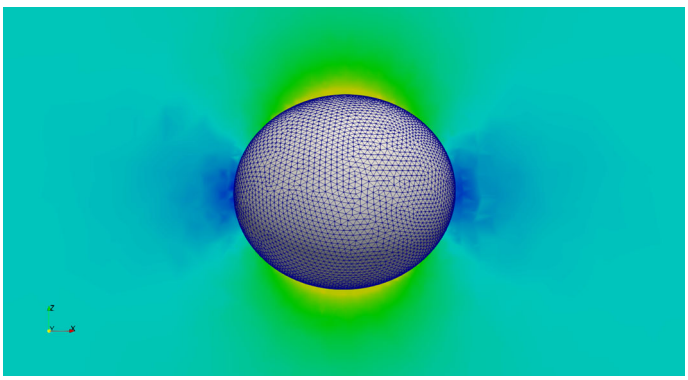

Fig. 6 FEM results: displacement field (scale factor: 5×10^3) of the steel and the magnetic flux on the cut shown with the same color code as in Fig. 5

applied by the domain boundary condition and the numerical value is changed by sphere's magnetization. The numerical solution is adequate; but there is a mismatch caused by the employed boundary conditions for the displacement field. The solution of the displacement field is strongly dependent on the clamped nodes within the inner sphere of R_{BC}.

The displacement field is solved simultaneously with the electromagnetic potentials such that the displacement boundary condition affects all solutions. The order of the displacements is in the range of μm, the result is scaled 5 000 times and shown in Fig. 6. The displacement field is qualitatively correct, see Fig. 3. By choosing MINKOWSKI's momentum, we obtain a shortening along the magnetic field leading to a widening along x-axis. We present the radial component along the radius at two distinct positions of $\theta = \{0, \pi/2\}$. Because of the azimuthal symmetry, this comparison is sufficient for obtaining a clear picture of the accuracy. Choosing $\theta = 0$ corresponds to u_z along z-axis. Analogously, setting $\theta = \pi/2$ is u_x along x-axis. Both are the radial components such that we use Eq. $(39)_1$ for comparison. Boundary condition's effect is clearly shown in

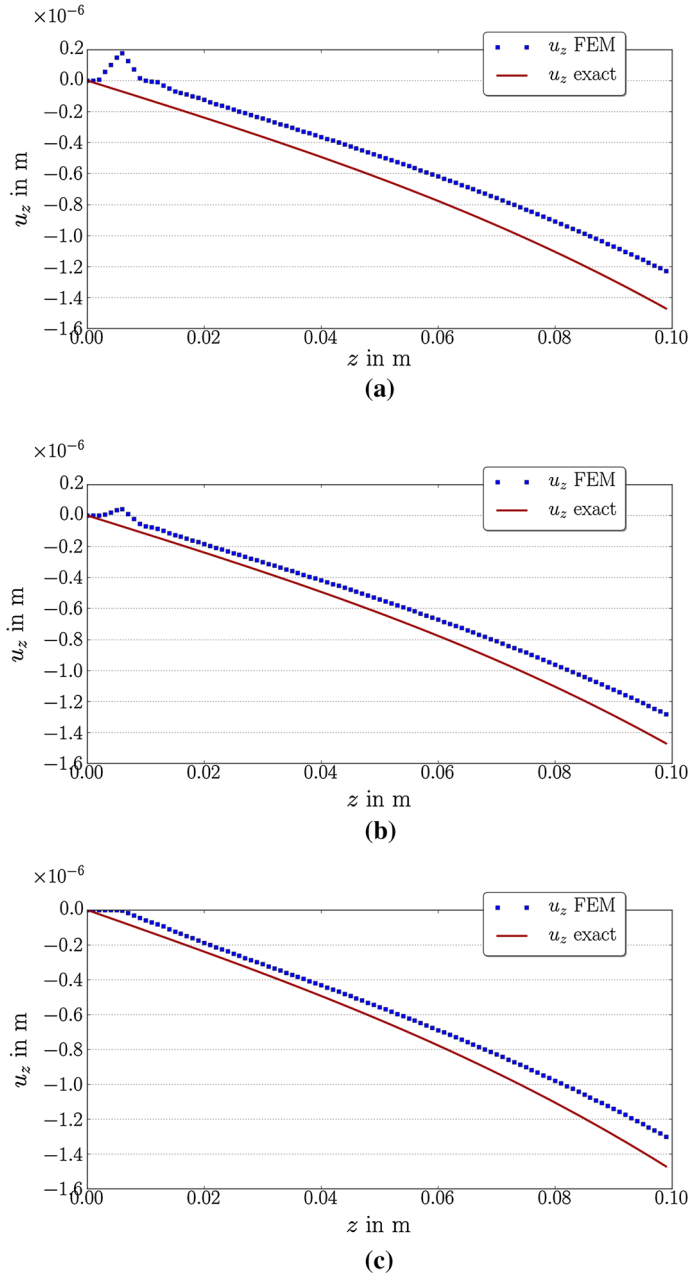

Fig. 7 Displacement field from the FEM shown as dots and the corresponding closed-form solution as continuous (red) line, along z-axis meaning r at $\theta = 0$. **a** $R_{\mathrm{BC}} = 5\,\mathrm{mm}$. **b** $R_{\mathrm{BC}} = 7.5\,\mathrm{mm}$. **c** $R_{\mathrm{BC}} = 10\,\mathrm{mm}$ (color figure online)

Figs. 7 and 8. As smaller R_{BC} gets, the singularity at the origin becomes more dominant leading to a perturbed solution near the boundary condition. Bigger R_{BC} generates a more reliable result; however, in this case the shift at the origin prevents the possible accuracy to be attained. In both cases, the numerical method converges to the solution, we present here a comparison with the converged solutions. The boundary condition is starkly minimalistic, in a possible experimental setup even a more complicated condition will be applied.

The radial symmetry as assumed in the closed-form solution is captured by the numerical results. The jump on the interface is represented correctly without using any special elements or a layered mesh on the interface, which shows the strength of the implementation of the balance equations on the singular surfaces into the weak form.

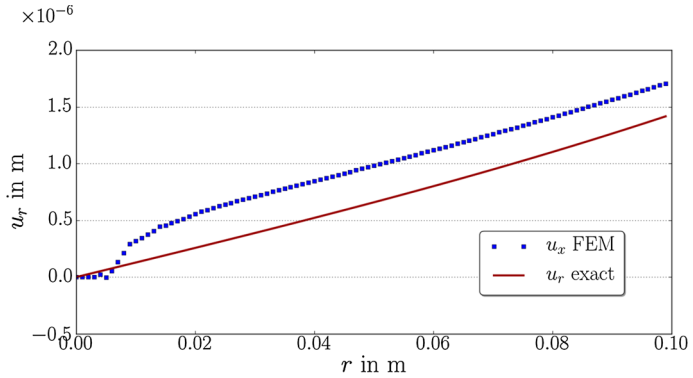

(a)

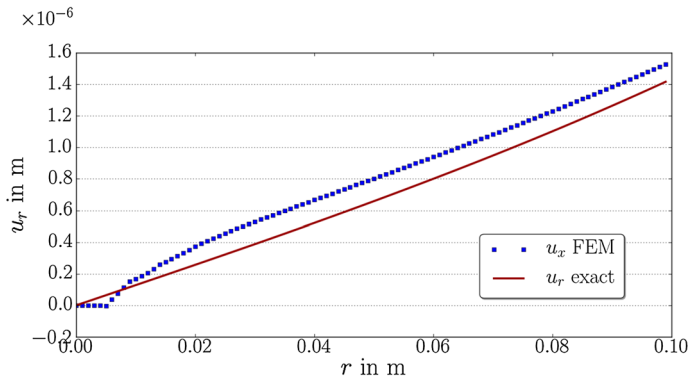

(b)

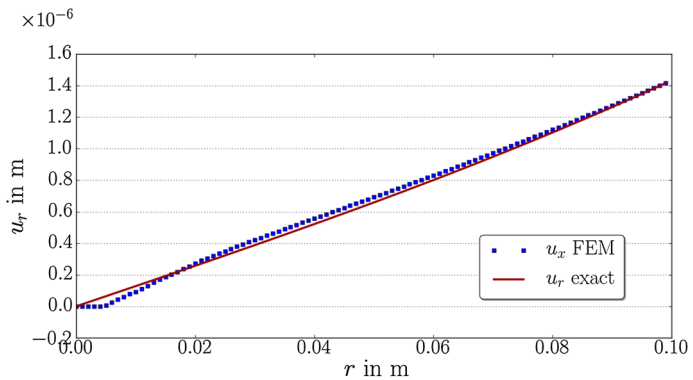

(c)

Fig. 8 Displacement field from the FEM shown as dots and the corresponding closed-form solution as continuous (red) line, along x-axis denoted by r at $\theta = \pi/2$. **a** $R_{\mathrm{BC}} = 5\,\mathrm{mm}$. **b** $R_{\mathrm{BC}} = 7.5\,\mathrm{mm}$. **c** $R_{\mathrm{BC}} = 10\,\mathrm{mm}$ (color figure online)

Conclusions

For determining the deformation of bodies due to electromagnetic fields, a monolithic numerical implementation has been examined by comparing it to a closed-form solution. Several simplifications lead to an analytic solution for a spherical continuum body being deformed by a homogeneous magnetic field. The magnetic flux possesses a jump between the continuum body and surrounding air. Such a jump between two materials is challenging to calculate accurately. Instead of solving the magnetic flux directly, we introduce potentials and solve them by using continuous elements. The derivative of the vector potential accurately represents the jump on the interface even in the case of a relatively coarse mesh on the interface. By using LORENZ gauge as well as

jump conditions, we have obtained the weak form that is computed by using standard finite elements. Without using any special elements, we have shown fairly accurate results for a magnetically polarized material in a constant external magnetic flux being deformed by the electromagnetic stress.

Acknowledgements B. E. Abali's work was partly supported by a grant from the Daimler and Benz Foundation.

References

1. Abali, B.E., Queiruga, A.F.: Theory and computation of electromagnetic fields and thermomechanical structure interaction for systems undergoing large deformations (2018). ArXiv preprint arXiv:1803.10551
2. Abali, B.E.: Computational Reality, Solving Nonlinear and Coupled Problems in Continuum Mechanics. Advanced Structured Materials. Springer, Berlin (2016)
3. Abali, B.E.: Technical University of Berlin, Institute of Mechanics, Chair of Continuum Mechanics and Material Theory, Computational Reality. http://www.lkm.tu-berlin.de/ComputationalReality/ (2016)
4. Abali, B.E., Reich, F.A.: Thermodynamically consistent derivation and computation of electro-thermo-mechanical systems for solid bodies. Comput. Methods Appl. Mech. Eng. **319**, 567–595 (2017)
5. Andreaus, U., dell'Isola, F., Porfiri, M.: Piezoelectric passive distributed controllers for beam flexural vibrations. Modal Anal. **10**(5), 625–659 (2004)
6. Arnold, D.N., Logg, A.: Periodic table of the finite elements. SIAM News **47**(9), 212 (2014)
7. Barchiesi, E., Spagnuolo, M., Placidi, L.: Mechanical metamaterials: a state of the art. Math. Mech. Solids (2018). https://doi.org/10.1177/1081286517735695
8. Barnett, S.M.: Resolution of the Abraham-Minkowski dilemma. Phys. Rev. Lett. **104**(7), 070401 (2010)
9. Baumanns, S., Clemens, M., Schops, S.: Structural aspects of regularized full maxwell electrodynamic potential formulations using fit. In: Proceedings of 2013 URSI International Symposium on Electromagnetic Theory (EMTS), pp. 1007–1010. IEEE (2013)
10. Benjeddou, A.: Advances in piezoelectric finite element modeling of adaptive structural elements: a survey. Comput. Struct. **76**(1), 347–363 (2000)
11. Bethune-Waddell, M., Chau, K.J.: Simulations of radiation pressure experiments narrow down the energy and momentum of light in matter. Rep. Prog. Phys. **78**(12), 122401 (2015)
12. Bossavit, A.: Whitney forms: a class of finite elements for three-dimensional computations in electromagnetism. IEE Proc. A (Phys. Sci. Meas. Instrum. Manag. Educ. Rev.) **135**(8), 493–500 (1988)
13. Ciarlet Jr., P., Zou, J.: Fully discrete finite element approaches for time-dependent Maxwell's equations. Numer. Math. **82**(2), 193–219 (1999)
14. de Groot, S.R., Mazur, P.: Non-equilibrium thermodynamics. Dover Publications, New York (1984)
15. Del Bufalo, G., Placidi, L., Porfiri, M.: A mixture theory framework for modeling the mechanical actuation of ionic polymer metal composites. Smart Mater. Struct. **17**(4), 045010 (2008)
16. Del Vescovo, D., Giorgio, I.: Dynamic problems for metamaterials: review of existing models and ideas for further research. Int. J. Eng. Sci. **80**, 153–172 (2014)
17. dell'Isola, F., Steigmann, D., Della Corte, A.: Synthesis of fibrous complex structures: designing microstructure to deliver targeted macroscale response. Appl. Mech. Rev. **67**(6), 060804 (2015). https://doi.org/10.1115/1.4032206
18. Demkowicz, L.: Computing with hp-adaptive Finite Elements: Volume 1 One and Two Dimensional Elliptic and Maxwell Problems. CRC Press, Boca Raton (2006)
19. Erbts, P., Hartmann, S., Düster, A.: A partitioned solution approach for electro-thermo-mechanical problems. Arch. Appl. Mech. **85**(8), 1075–1101 (2015)
20. Eremeyev, V.A., Nasedkin, A.V., Solov'yev, A.N.: Partitioned schemes of the finite-element method for dynamic problems of acoustoelectroelasticity. J. Appl. Math. Mech. **64**(3), 367–377 (2000)
21. Ericksen, J.L.: On formulating and assessing continuum theories of electromagnetic fields in elastic materials. J. Elast. **87**(2–3), 95–108 (2007)
22. Gillette, A., Rand, A., Bajaj, C.: Construction of scalar and vector finite element families on polygonal and polyhedral meshes. Comput. Methods Appl. Math. **16**(4), 667–683 (2016)
23. Giorgio, I., Galantucci, L., Corte, A.D., Vescovo, D.D.: Piezo-electromechanical smart materials with distributed arrays of piezoelectric transducers: current and upcoming applications. Int. J. Appl. Electromagn. Mech. **47**(4), 1051–1084 (2015)
24. Glane, S., Reich, F.A., Müller, W.H.: Modeling of non-ideal hard permanent magnets with an affine-linear model, illustrated for a bar and a horseshoe magnet. Contin. Mech. Thermodyn. **29**, 1313–1333 (2017)
25. GNU Public. Gnu general public license. http://www.gnu.org/copyleft/gpl.html (2007)
26. Griffiths, D.J.: Resource letter EM-1: electromagnetic momentum. Am. J. Phys. **80**(1), 7–18 (2012)
27. Griffiths, D.J., College, R.: Introduction to Electrodynamics, vol. 3. Prentice Hall, Upper Saddle River (1999)
28. Hachkevych, O.R., Terlets'kyi, R.F.: Models of thermomechanics of magnetizable and polarizable conducting deformable solids. Mater. Sci. **40**(3), 320–336 (2004)
29. Hiramatsu, Y., Oka, Y.: Determination of the tensile strength of rock by a compression test of an irregular test piece. Int. J. Rock Mech. Min. Sci. Geomech. Abstr. **3**(2), 89–90 (1966)
30. Jones, D.S.: The Theory of Electromagnetism. Pergamon, New York (1964)
31. Li, J.: Numerical convergence and physical fidelity analysis for Maxwell's equations in metamaterials. Comput. Methods Appl. Mech. Eng. **198**(37), 3161–3172 (2009)

32. Lorentz, H.A.: Zittungsverlagen akad. van wettenschappen 1, 74 (Nov. 26, 1892); versuch einer theorie der elektrischen und optischen erscheinungen in bewegten körpern, brill, leiden, 1895. Proc. Acad. Sci. (Amsterdam) (Engl. version), 6:809 (1904)
33. Low, F.E.: Classical Field Theory: Electromagnetism and Gravitation. Wiley-VCH, Weinheim (2004)
34. Mansuripur, M.: Resolution of the Abraham–Minkowski controversy. Opt. Commun. **283**(10), 1997–2005 (2010)
35. Misra, A., Poorsolhjouy, P.: Identification of higher-order elastic constants for grain assemblies based upon granular micromechanics. Math. Mech. Complex Syst. **3**(3), 285–308 (2015)
36. Müller, I.: Thermodynamics. Pitman Publishing, London (1985)
37. Nédélec, J.-C.: Mixed finite elements in R3. Numer. Math. **35**(3), 315–341 (1980)
38. Obukhov, Y.N.: Electromagnetic energy and momentum in moving media. Annalen der Physik **17**(9–10), 830–851 (2008)
39. Placidi, L., Andreaus, U., Corte, A.D., Lekszycki, T.: Gedanken experiments for the determination of two-dimensional linear second gradient elasticity coefficients. Zeitschrift für angewandte Mathematik und Physik **66**(6), 3699–3725 (2015)
40. Queiruga, A.F., Zohdi, T.I.: Formulation and numerical analysis of a fully-coupled dynamically deforming electromagnetic wire. Comput. Methods Appl. Mech. Eng. **305**, 292–315 (2016)
41. Raviart, P.-A., Thomas, J.-M.: A mixed finite element method for 2-nd order elliptic problems. In: Mathematical Aspects of Finite Element Methods, pp. 292–315. Springer (1977)
42. Reich, F.A.: Coupling of continuum mechanics and electrodynamics: an investigation of electromagnetic force models by means of experiments and selected problems. Ph.D. thesis, TU Berlin (2017)
43. Reich, F.A., Stahn, O., Müller, W.H.: A review of electrodynamics and its coupling with classical balance equations. In: Advanced Problems in Mechanics, International Summer School–Conference Proceedings, pp. 367–376. Institute for Problems in Mechanical Engineering, 22 June 2015–27 June 2015, St. Petersburg, Russia (2015)
44. Steigmann, D.J.: On the formulation of balance laws for electromagnetic continua. Math. Mech. Solids **14**(4), 390–402 (2009)
45. Svendsen, B., Chanda, T.: Continuum thermodynamic formulation of models for electromagnetic thermoinelastic solids with application in electromagnetic metal forming. Contin. Mech. Thermodyn. **17**(1), 1–16 (2005)
46. Turco, E.: Tools for the numerical solution of inverse problems in structural mechanics: review and research perspectives. Eur. J. Environ. Civ. Eng. **21**(5), 509–554 (2017)
47. Vidal, P., D'Ottavio, M., Thaïer, M.B., Polit, O.: An efficient finite shell element for the static response of piezoelectric laminates. J. Intell. Mater. Syst. Struct. **22**(7), 671–690 (2011)
48. Zohdi, T.I.: Electromagnetic Properties of Multiphase Dielectrics: A Primer on Modeling, Theory and Computation, vol. 64. Springer, Berlin (2012)